Acoustic modal analysis and control in *w*-shaped triple-layer optical fibers with highly-germanium-doped core and F-doped inner cladding

Weiwen Zou*, Zuyuan He, and Kazuo Hotate

Department of Electronic Engineering, The University of Tokyo, Tokyo 113-8656, Japan
**Corresponding author: zou@sagnac.t.u-tokyo.ac.jp*

Abstract: The numerical study of acoustic modal properties in *w*-shaped optical fibers with high-delta germanium-doped core and F-doped inner cladding (F-HDF) is demonstrated. The cutoff conditions of acoustic modes in the F-HDF show opposite behaviors in contrast with those of optical ones because F-doped inner cladding contributes differently to acoustic and optical waveguides. The acoustic dispersion characteristics vary to a great extent with respect to the location of the acoustic modes in the fiber's core or in the fiber's inner cladding. The resonance frequency spacing between neighboring acoustic modes is theoretically and experimentally found to have a quadratic relation to the core's germanium concentration. We also investigate the critical conditions to move high-order acoustic modes into the F-doped inner cladding and validate the optimal feasibility of employing L_{01} and L_{03} acoustic modes to fiber-optic Brillouin-based discriminative sensing of strain and temperature.

OCIS codes: (290.5830) Scattering, Brillouin; (060.2310) Fiber optics; (060.2270) Fiber characterization; (060.2280) Fiber design and fabrication; (060.2370) Fiber optics sensors.

References and links

1. A. Kobyakov, S. Kumar, D. Q. Chowdhury, A. B. Ruffin, M. Sauer, and S. R. Bickham, "Design concept for optical fibers with enhanced SBS threshold," Opt. Express **13**, 5338–5346, 2005.
2. M. J. Li, S. Li and D. A. Nolan, "Nonlinear fibers for signal processing using Kerr effects," J. Lightwave Technol. **23**, 3606–3614, 2005.
3. S. R. Bickham, X. Chen, M. J. Li, and D. T. Walton, "High SBS threshold optical fiber with fluorine dopant," U. S. Patent 7228039 (June 2007).
4. I. Flammer, "Optical fiber with reduced stimulated Brillouin scattering," U. S. Patent application, 2007/0081779 (April 2007)
5. M. Nikles, L. Thevenaz, P. A. Robert, "Simple distributed fiber sensor based on Brillouin gain spectrum analysis," Opt. Lett. **21**, 738–740, 1996.
6. K. Hotate and M. Tanaka, "Distributed fiber Brillouin strain sensing with 1-cm spatial resolution by correlation-based continuous-wave technique," IEEE Photon. Technol. Lett. **14**, 179–181, 2002.
7. W. Zou, Z. He, M. Kishi, and K. Hotate, "Stimulated Brillouin scattering and its dependences on temperature and strain in a high-delta optical fiber with F-doped depressed inner cladding," Opt. Lett. **32**, 600–602, 2007.
8. A. Yeniay, J. M. Delavaux, and J. Toulouse, "Spontaneous and stimulated Brillouin scattering gain spectra in optical fibers," J. Lightwave Technol. **20**, 1425–1432, 2002.
9. M. Monerie, "Propagation in doubly clad single-mode fibers," IEEE J. Quantum Electron. **QE-18**, 535–542, 1982.
10. B. J. Ainslie, K. J. Beales, C. R. Day, and J. D. Rush, "The design and fabrication of monomode optical fiber," IEEE J. Quantum Electron. **QE-18**, 514–523, 1982.

#96317 - $15.00 USD Received 16 May 2008; revised 18 Jun 2008; accepted 18 Jun 2008; published 23 Jun 2008

11. Y. Koyamada, S. Sato, S. Nakamura, H. Sotobayashi, and W. Chujo, "Simulating and designing Brillouin gain spectrum in single-mode fibers," J. Lightwave Technol. **22**, 631–639, 2004.
12. Y. Y. Huang, A. Sarkar, and P. C. Schultz, "Relationship between composition, density and refractive index for germania silica glasses," J. Non-Cryst. Solid. **27**, 29–37, 1978.
13. Y. Park, K. Oh, U. C. Paek, D. Y. Kim, and C. R. Kurkjian, "Residual stresses in a doubly clad fiber with depressed inner cladding (DIC)," J. Lightwave Technol. **17**, 1823–1834, 1999.
14. W. Zou, Z. He, A. D. Yablon, and K. Hotate, "Dependence of Brillouin frequency shift in optical fibers on draw-induced residual elastic and inelastic strains," IEEE Photon. Technol. Lett. **19**, 1389–1391, 2007.
15. T. Mito, S. Fujino, H. Takeba, K. Morinaga, S. Todoroki, and S. Sakaguchi, "Refractive index and material dispersions of multi-component oxide glasses," J. Non-Cryst. Solid. **210**, 155–162, 1997.
16. C. Su, "Eigenproblems of radially inhomogeneous optical fibers from the scalar formulation," IEEE J. Quantum Electron. **QE-10**, 1554–1557, 1985.
17. E. Peral and A. Yariv, "Degradation of modulation and noise characteristics of semiconductor lasers after propagation in optical fiber due to shift induced by stimulated Brillouin scattering," IEEE J. Quantum Electron. **35**, 1185–1195, 1999.
18. W. Zou, Z. He, and K. Hotate, "Two-dimensional finite element modal analysis of Brillouin gain spectra in optical fibers," IEEE Photon. Technol. Lett. **18**, 2487–2489, 2006.

1. Introduction

Stimulated Brillouin scattering (SBS) phenomenon in optical fibers is generated from the nonlinear interaction among counter-propagating optical waves and thermally-initialized acoustic waves that are intensified by the optical waves' interference via the electro-striction effect. Meanwhile, SBS phenomenon can also happen when only a strong optical wave is launched into optical fibers with optical power beyond the so-called threshold value. The SBS phenomenon in optical fibers induces a big trouble to optical fiber communications [1-4] but provides a good opportunity to build up novel fiber-optic sensors [5, 6].

The counter-propagating optical waves have frequency deviations from each other that are determined by the resonance frequencies of the existing acoustic modes in optical fibers. The resonance frequency of the main-peak Brillouin gain spectrum (BGS) generated from the fundamental L_{01} acoustic mode, that is, Brillouin frequency shift (BFS), has a linear relationship to applied strain or temperature change. The linear relationship has been used to build a type of fully-distributed fiber-optic Brillouin sensors [5, 6] for smart materials and structures. However, Brillouin-based sensors encounter a physical difficulty in discriminating the response to strain from that to temperature. To solve this problem, a *w*-shaped triple-layer single-mode optical fiber structure with a high-delta GeO_2-doped core and F-doped inner cladding (F-HDF) was recently proposed and investigated [7]. Owing to the possible variance of F-doped silica from GeO_2-doped silica, four resonance frequencies in that F-HDF from various L_{0l} longitudinal acoustic modes hold different dependence behaviors to strain and temperature. The combination of 1st-order L_{01} together with 4th-order L_{04} modes provided a lowest discriminative error. This is because the L_{04} acoustic mode locates nearest to the F-doped inner cladding although still in the GeO_2-doped core. It was expected that the discriminative sensing performance could be enhanced if high-order acoustic mode, such as L_{02} or L_{03} mode, was moved into the F-doped inner cladding with comparable Brillouin gain in contrast with the fundamental L_{01} acoustic mode that is always confined in the GeO_2-doped core.

In this paper, we demonstrate the theoretical analysis and control of acoustic modal properties in the F-HDF. The cutoff conditions of acoustic modes and the acoustic dispersion characteristics are thoroughly studied, which clarify the recently observed abnormal Brillouin scattering phenomenon in an F-HDF [8]. We also investigate the critical conditions to move high-order acoustic modes into the F-doped inner cladding. The optimal feasibility of utilizing L_{01} and L_{03} acoustic modes for discriminative sensing is verified by setting fiber parameters to let L_{03} mode below its critical condition while just close to its cutoff condition.

#96317 - $15.00 USD Received 16 May 2008; revised 18 Jun 2008; accepted 18 Jun 2008; published 23 Jun 2008

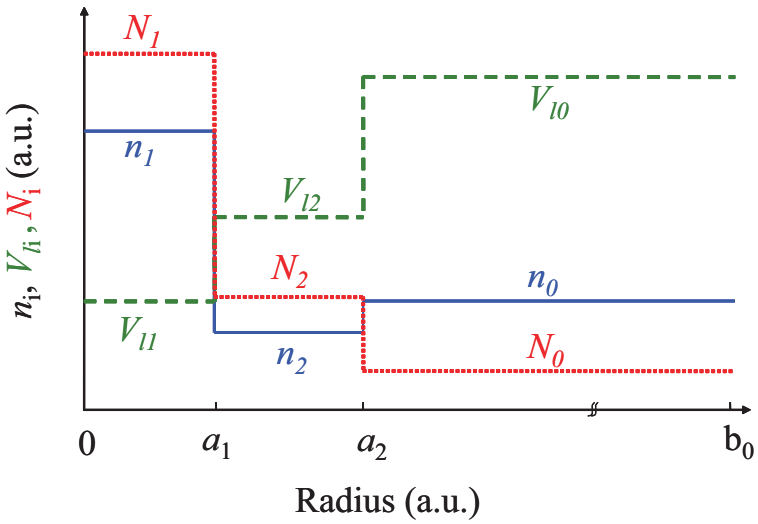

Fig. 1. Schematic diagrams of transverse profiles of refractive index (n_i), longitudinal acoustic velocity (V_{li}), and longitudinal acoustic index (N_i) in an F-HDF. The subscripts i = 1, 2, 0 correspond to the core, inner cladding and outer cladding, respectively.

2. Mathematical principles

2.1. *Optical refractive index and longitudinal acoustic index*

The F-HDF includes triple layers: GeO_2-doped core ($r \leq a_1$), F-doped inner cladding ($a_1 \leq r \leq a_2$) and pure-silica outer cladding ($a_2 \leq r \leq b_0$) where r is a radial coordinate in the cylindrical optical fiber, a_1 the core radius, a_2 the outer radius of the inner cladding and b_0 the outer radius of the outer cladding (i.e., $\sim$62.5 μm). The optical properties of F-HDF structure such as the optical cutoff condition and the modified optical dispersion properties have been comprehensively reported by Monerie [9] and the fabrication of the F-HDF has been demonstrated in [10].

Figure 1 schematically illustrates the refractive index n_i profile (solid curve) and the longitudinal acoustic velocity V_{li} profile (dashed curve) of the F-HDF where the subscripts i = 1, 2, 0 correspond to the core, inner cladding and outer cladding, respectively. In this study, we introduce a longitudinal acoustic index N_i, as also plotted in Fig. 1 (dotted curve), which is defined as the ratio of the longitudinal acoustic velocity of pure silica (V_{l0}, 5944 m/s [11]) to that of GeO_2-doped or F-doped silica (V_{li}):

$$N_i = \frac{V_{l0}}{V_{li}}. \tag{1}$$

From Fig. 1, one can qualitatively know that the F-doped inner-cladding layer depresses the optical waveguide but enhances the acoustic waveguide, which has been preliminarily clarified in [7]. The n_i and N_i are dependent on the ith-layer dopant concentrations:

$$n_i = n_0(1 + 1.0 \times 10^{-3} w_1 - 3.3 \times 10^{-3} w_2), \tag{2}$$

$$N_i = N_0(1 + 7.2 \times 10^{-3} w_1 + 2.7 \times 10^{-2} w_2), \tag{3}$$

where w_1 and w_2 are the concentrations of GeO_2 and F in units of molecular percent ($mol\%$) and weight percent ($wt\%$), respectively. It is worth noting that the above relationships are basically referred to [11] but the unit of GeO_2 concentration w_1 is thought to be $mol\%$ rather than $wt\%$

#96317 - $15.00 USD Received 16 May 2008; revised 18 Jun 2008; accepted 18 Jun 2008; published 23 Jun 2008

according to Ref. [12] and therein references in Ref. [11]. We also note that the influence of the residual stress during fiber fabrication [13] is not taken into account in this study although SBS properties could be modified to some extent by the residual stress [14]. The indices n_0 = 1.444 in 1.55-μm region [15] and N_0 = 1.0 correspond to pure silica.

2.2. Optical scalar-wave equation

We redefine the physical core and the physical inner cladding of an F-HDF as the calculated core region and the physical outer cladding as the calculated cladding region for the purpose of two-dimensional finite-element-method (2D-FEM) modal analysis of its BGS. The optical mode in the redefined calculated core region satisfies the following normalized scalar-wave equation:

$$\nabla_a^2 E_i + (\mathrm{v}_{op}^2 P_{op}^2 - W_{op}^2) E_i = 0, \tag{4}$$

where $\nabla_a^2 = \partial^2/\partial x'^2 + \partial^2/\partial y'^2$ is the transverse Laplacian in a coordinate normalized to the outer radius of the inner cladding a_2 (i.e., $x' = x/a_2, y' = y/a_2$); E_i, the transverse electric field of the fundamental LP_{01} optical mode [i.e., $E_x(x',y')$ for HE_{11}^x mode and $E_y(x',y')$ for HE_{11}^y mode]. v_{op}, P_{op}, and W_{op} are the optical normalized frequency, the normalized refractive index distribution, and the normalized optical transverse wave number, respectively, which are given by

$$\mathrm{v}_{op} = k_0 a_1 \sqrt{n_1^2 - n_0^2},\ P_{op} = \frac{a_2}{a_1} \frac{\sqrt{n_i(r')^2 - n_0^2}}{\sqrt{n_1^2 - n_0^2}},\ W_{op} = k_0 a_2 \sqrt{n_{eff}^2 - n_0^2}, \tag{5}$$

where k_0 (= $2\pi/\lambda_0$) is the free-space optical wave number with λ_0 (= 1.549 μm in this study) the optical wavelength in vacuum, $n_i(r')$ with $r' = r/a_2$ is the radial refractive index distribution in the normalized coordinates, and n_{eff} is the optical effective refractive index that determines the effective propagation constant $\beta_{op} = k_0 n_{eff}$.

The optical boundary condition at the interface between the calculated core region and the calculated cladding region can be expressed as [16]:

$$\overrightarrow{n} \cdot \nabla_a E_i + \frac{W_{op} \cdot K_1(W_{op})}{K_0(W_{op})} E_i = 0, \tag{6}$$

where $\overrightarrow{n}$ is the outward pointing normal on the boundary and $K_m(W_{op})$ is the mth-order second-kind modified Bessel function.

2.3. Acoustic scalar-wave equation

The longitudinal lth-order L_{0l} acoustic displacement field distributions (u_z) follow the eigenvalue equation [1, 17]:

$$\nabla^2 u_z + (\frac{\omega_{ac}^{(l)}}{V_{l1}^2} - \beta_{ac}^2) u_z = 0, \tag{7}$$

where $\nabla^2 = \partial^2/\partial x^2 + \partial^2/\partial y^2$, β_{ac} is the propagation constant of the longitudinal acoustic modes decided by the Bragg-like phase-matching condition as $\beta_{ac} = 2\beta_{op}$, and $\omega_{ac}^{(l)}$ is the lth-order angular resonance frequency that is relative to β_{ac} and the effective lth-order longitudinal acoustic velocity $V_a^{(l)}$ as $\omega_{ac}^{(l)} = V_a^{(l)} \beta_{ac}$.

Taken into account the defined acoustic indices in Eq. (1), the above acoustic scalar-wave equation in the calculated core region can be modified into the similar scalar-wave equation to Eq. (4) in the normalized coordinates:

$$\nabla_a^2 u_z + [\mathrm{v}_{ac}^2 P_{ac}^2 - W_{ac}^2 \cdot N_i(r')^2] u_z = 0, \tag{8}$$

#96317 - $15.00 USD Received 16 May 2008; revised 18 Jun 2008; accepted 18 Jun 2008; published 23 Jun 2008

where v_{ac}, P_{ac}, and W_{ac} denote the normalized acoustic frequency, the normalized acoustic index distribution, and the normalized acoustic transverse wavenumber, respectively, which are defined by:

$$v_{ac} = \beta_{ac} a_1 \sqrt{N_1^2 - N_0^2},\ P_{ac} = \frac{a_2}{a_1} \frac{\sqrt{N_i(r')^2 - N_0^2}}{\sqrt{N_1^2 - N_0^2}},\ W_{ac} = \beta_{ac} a_2 \sqrt{1 - \frac{1}{N_{eff}^2}}, \tag{9}$$

where $N_i(r')$ is the longitudinal acoustic index distribution and $N_{eff}^{(l)}$ is the effective acoustic index of the longitudinal lth-order L_{0l} acoustic mode that determines the L_{0l} mode's effective acoustic velocity as $V_a^{(l)} = V_{l0}/N_{eff}^{(l)}$. As follows, the lth-order resonance frequency $\nu_{ac}^{(l)} = \beta_{ac} \cdot V_a^{(l)}/2\pi$ in the F-HDF's BGS can be expressed as:

$$\nu_{ac}^{(l)} = \frac{2V_{l0}}{\lambda_o} \frac{n_{eff}}{N_{eff}^{(l)}}. \tag{10}$$

The boundary condition of the longitudinal L_{0l} acoustic mode also satisfies the Eq. (6) except for the substitution of the acoustic eigenvalue W_{ac} for the optical eigenvalue W_{op}.

2.4. Numerical method

The 2D-FEM modal analysis [18] is used to solve Eq. (4) for optical modes and Eq. (8) for acoustic modes in the F-HDF, respectively, both based on the boundary equation of Eq. (6). Consequently, the lth-order L_{0l} acoustic resonance frequency in Eq. (10) is quantified; the lth-order Brillouin gain (g_l) is evaluated which is inversely proportional to the acousto-optic effective area $A_{eff}^{ao(l)}$ [1] as

$$A_{eff}^{ao(l)} = [\frac{< E_i^2 >}{< u_z^{(l)} E_i^2 >}]^2 < u_z^{(l)2} >, \tag{11}$$

where the inner product $< f >= \int\int f(x',y')\mathrm{d}x'\mathrm{d}y'$ is over all the calculated core and cladding regions.

3. Modal analysis and modal control

3.1. Cutoff conditions

From the definitions of Eq. (5) and Eq. (9), the ratio v_{ac}/v_{op} can be deduced to be

$$v_{ac}/v_{op} = 2n_{eff} \frac{\sqrt{N_1^2 - N_0^2}}{\sqrt{n_1^2 - n_0^2}}, \tag{12}$$

which is relative not only to n_{eff} but also to the GeO_2 concentration w_1 since n_1 and N_1 are both proportional to w_1 as given in Eq. (2) and Eq. (3), respectively.

Our numerical result, as illustrated in Fig. 2, shows that v_{ac} is 5.37 to 6.00 times of v_{op}, which means that the longitudinal acoustic modes sense better confinement than the optical mode. This characteristic is responsible for the existence of multiple-peak BGS in a GeO_2-doped single-mode fiber (SMF) and even in the standard step-index SMF [18], and also responsible for the greatest acousto-optic overlapping efficiency (i.e., 100%) of the fundamental L_{01} acoustic mode among the multiple-peak BGS.

#96317 - $15.00 USD Received 16 May 2008; revised 18 Jun 2008; accepted 18 Jun 2008; published 23 Jun 2008

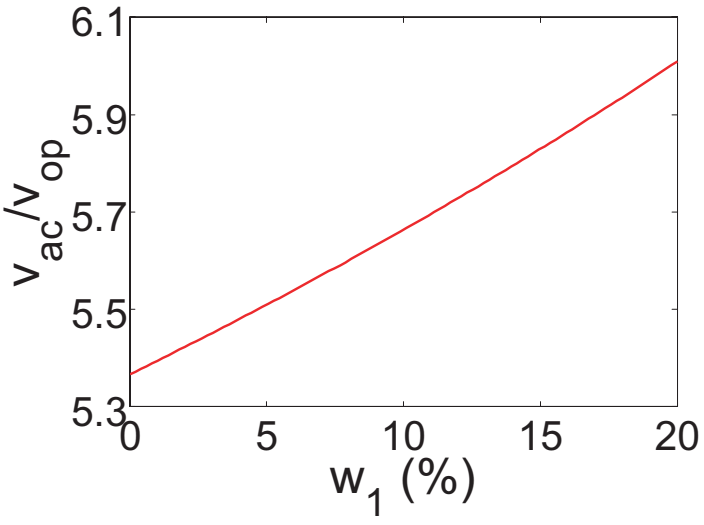

Fig. 2. Ratio of v_{ac}/v_{op} as a function of GeO_2 concentration in the physical core (w_1, in unit of *mol%*).

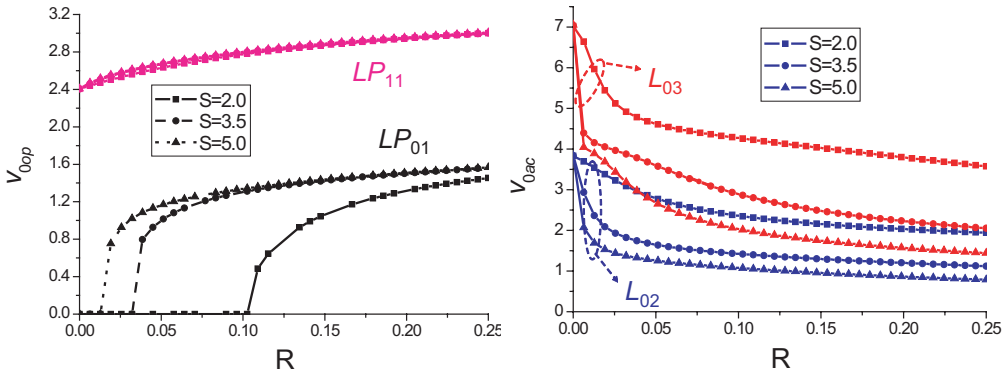

Fig. 3. (a) Optical cutoff v_{0op} and (b) acoustic cutoff v_{0ac} as functions of concentration ratio R for different radius ratio S.

The optical cutoff normalized frequencies v_{0op} for LP_{01} and LP_{11} modes are quantified at different concentration ratio $R = w_2/w_1$ and radius ratio $S = a_2/a_1$. To do that, the optical cutoff condition of $W_{op} = 0$ (i.e., $n_{eff} = n_0$) in Eq. (5) is preset for the boundary condition of Eq. (6) as follows:

$$\vec{n} \cdot \nabla_a E_i = 0, \vec{n} \cdot \nabla_a E_i + E_i = 0, \tag{13}$$

respectively, for LP_{01} or LP_{11}.

The optical cutoff characteristics after our numerical analysis are depicted in Fig. 3(a). The v_{0op} is increased when the concentration ratio R or radius ratio S is increased, and further the fundamental LP_{01} optical mode has a nonzero cutoff v_{0op}. Our results are in good agreement with previously-reported ones [9]. The physical reason is because the F-doped inner cladding depresses the optical waveguide as mentioned above in Fig. 1.

#96317 - $15.00 USD Received 16 May 2008; revised 18 Jun 2008; accepted 18 Jun 2008; published 23 Jun 2008

Similarly, we evaluate the longitudinal acoustic cutoff properties that are summarized in Fig. 3(b) for L_{02} or L_{03} acoustic mode. The cutoff v_{0ac} becomes reductive when the concentration ratio R or radius ratio S increases, which coincides with our previous estimation that F-doped inner cladding acts as an enhanced waveguide layer for acoustic modes [see Fig. 1].

3.2. *Acoustic dispersion properties*

We numerically solve the Eq. (8) for different v_{ac} at different concentration ratio R or radius ratio S to evaluate the dispersion curves of L_{0l} acoustic modes in the F-HDF which denote the relations between W_{ac}/S and v_{ac}.

The dispersion curves of L_{01} (blue solid curves), L_{02} (green dashed curves) and L_{03} (red dotted curves) acoustic modes for the concentration ratio $R = 0.05$ and the GeO_2 concentration $w_1 = 10\ mol\%$ are plotted in Fig. 4(a) where a cluster of curves in the same color corresponds to different radius ratios S (= 1.0, 2.0, 3.5, and 5.0 from right side to left side). Similarly, Fig. 4(b) denotes the corresponding acoustic dispersion curves at the same parameters as those of Fig. 4(a) except for $R = 0.10$. In Figs. 4(a) or (b), a black solid linear curve as a based line corresponds to the case when $N_{eff} = N_2$, which means that the acoustic mode is just cutoff at the interface between the physical core and the physical inner cladding.

A crossing point (A_l with l = 1, 2 or 3) between lth-order acoustic dispersion curve and the based line in Fig. 4 determines a critical value of $v_{c-ac}^{(l)}$. If v_{ac} is just below the $v_{c-ac}^{(l)}$ then $N_{eff}^{(l)} < N_2$, which means that the lth-order acoustic mode enters into the F-doped physical inner cladding; vice versa, the lth-order acoustic mode still exists in the GeO_2-doped physical core. For example, when $w_1 = 10\ mol\%$, $R = 0.05$ and $S = 1.5$, $v_{c-ac}^{(3)} = 8.12$ for the $3rd$-order L_{03} acoustic mode. Figure 5 illustrates our evaluated field distributions of the fundamental LP_{01} optical mode and all L_{0l} acoustic modes in the calculated core region for the above fiber parameters of w_1, R and S but at different acoustic v_{ac}. It can be clearly seen that when v_{ac} becomes smaller than $v_{c-ac}^{(3)}$ the L_{03} field enters more into the F-doped physical inner cladding.

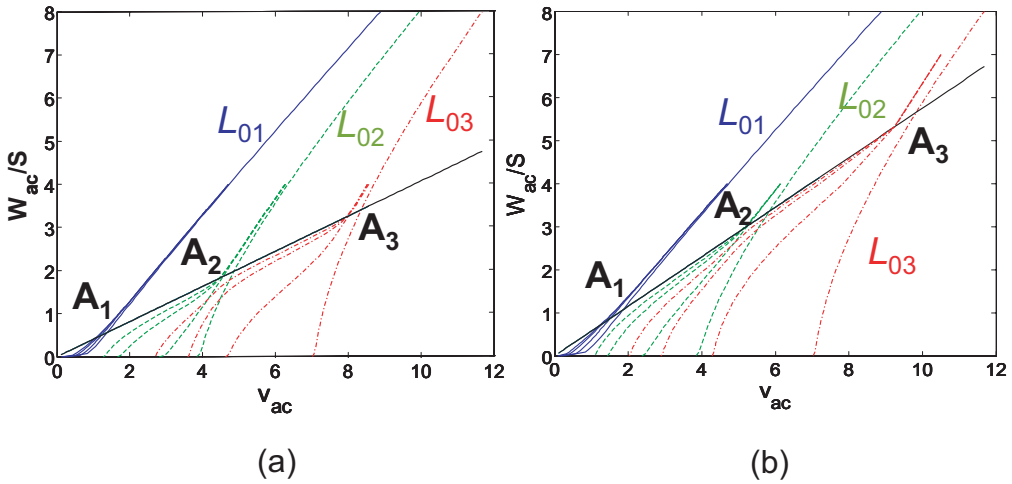

Fig. 4. Acoustic dispersion curves of W_{ac}/S as functions of v_{ac} for L_{01}, L_{02} and L_{03} modes, respectively, when $w_1 = 10\ mol\%$. (a) $R = 0.05$; (b) $R = 0.10$. The radius ratio S is 1.0, 2.0, 3.5 or 5.0 for the same-color cluster of curves from right to left. A_l point (l = 1, 2 or 3) depicts the crossing point of the based line with the dispersion curve of lth-order acoustic mode.

#96317 - $15.00 USD Received 16 May 2008; revised 18 Jun 2008; accepted 18 Jun 2008; published 23 Jun 2008

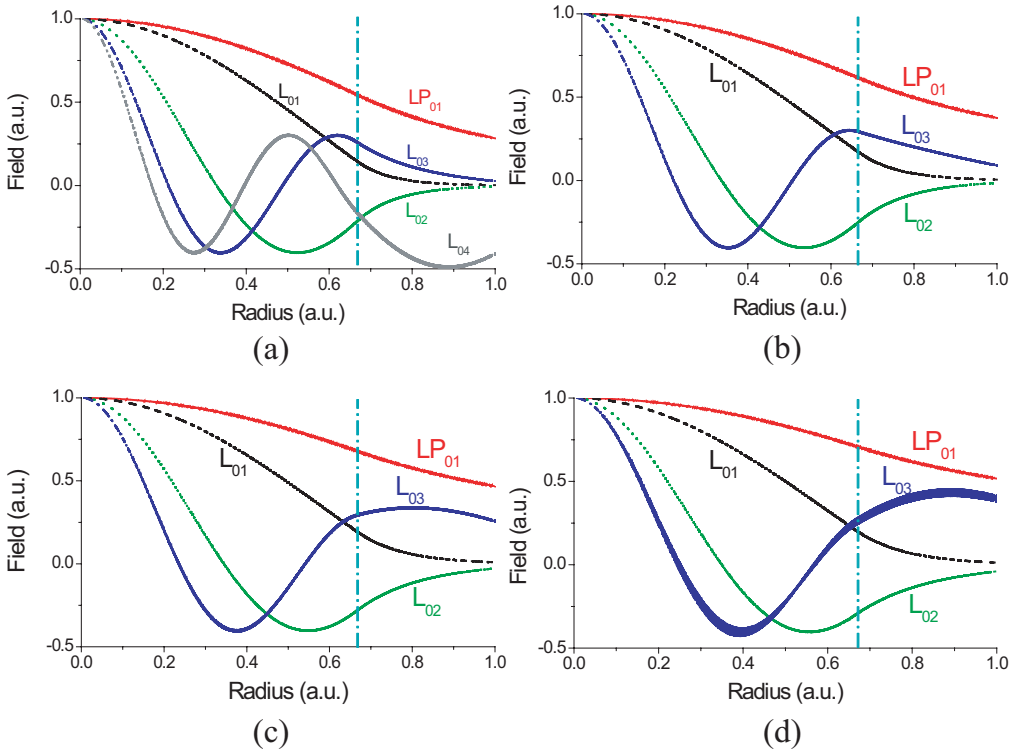

Fig. 5. Optical LP_{01} and acoustic L_{0l} field distributions in the calculated core region when $w_1 = 10$ *mol%*, $R = 0.05$ and $S = 1.5$. (a) $v_{ac} = 9.54 > v_{c-ac}^{(3)}$; (b) $v_{ac} = 8.12 = v_{c-ac}^{(3)}$; (c) $v_{ac} = 7.03 < v_{c-ac}^{(3)}$; (d) $v_{ac} = 6.53 < v_{c-ac}^{(3)}$. The dashed-dotted lines are used to separate the physical core and the physical inner cladding.

Comparing Fig. 4(a) against Fig. 4(b), we know that the critical value $v_{c-ac}^{(l)}$ is almost independent on the radius ratio S; however, it is sensitive to the concentration ratio R: when R is increased, it is correspondingly increased. These dependences can be further understood from Fig. 6 where the lth-order acoustic mode's critical value $v_{c-ac}^{(l)}$ and the $(l+1)$th-order acoustic mode's cutoff value $v_{0ac}^{(l+1)}$ are plotted together as functions of the concentration ratio R for different radius ratio S.

In fact, a starting point of lth-order acoustic dispersion curve from the horizontal axis in Fig. 4 corresponds to its cutoff value $v_{0ac}^{(l)}$. From it, we can clearly see that the cutoff value $v_{0ac}^{(l)}$ is reduced when the radius ratio S is increased, which means that the higher-order acoustic modes become more difficult to be cut off by the pure-silica outer cladding. Further, when the radius ratio S is increased, the parts of the dispersion curves below the based line become closer, which results in closer acoustic modes existing in the F-doped inner cladding. These analyzed properties can well explain the experimental observation in Ref. [8] where two groups of BGS were observed in that F-HDF: one group including two separate peaks is due to its location in the GeO_2-doped core but the other group including three closer peaks due to its location in the F-doped region. Figure 7 depicts our simulated BGS of the F-HDF demonstrated by Yeniay *et al*. [8], in which a dashed line is used to mark the two disparate groups of BGS existing in the GeO_2-doped core and the F-doped inner cladding, respectively.

Figure 8(a) illustrates the analyzed acoustic dispersion curves for two different w_1 of 3.65

#96317 - $15.00 USD Received 16 May 2008; revised 18 Jun 2008; accepted 18 Jun 2008; published 23 Jun 2008

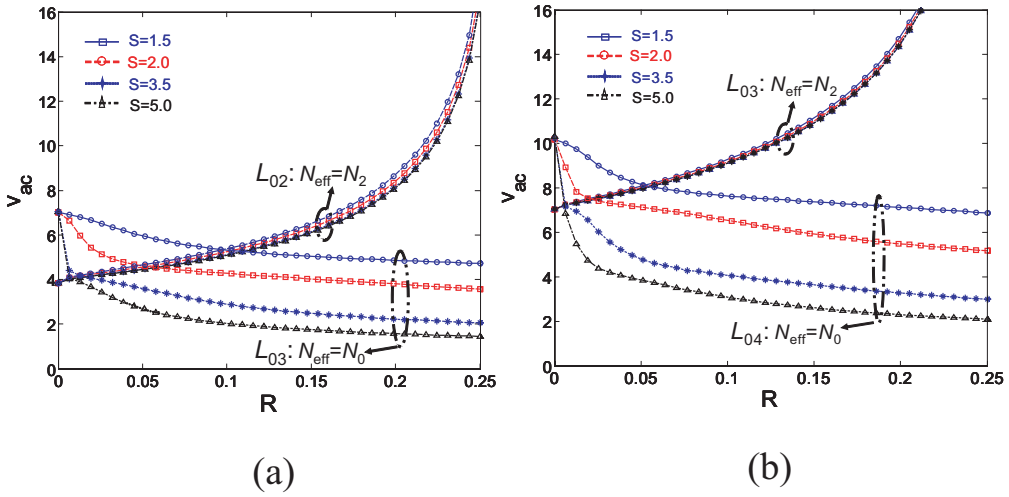

Fig. 6. Acoustic critical $v_{c-ac}^{(l)}$ of lth-order mode and acoustic cutoff $v_{0ac}^{(l+1)}$ of $(l+1)$th-order mode as functions of concentration ratio R for different radius ratio S when w_1 = 10 *mol%*. (a) l = 2; (b) l = 3.

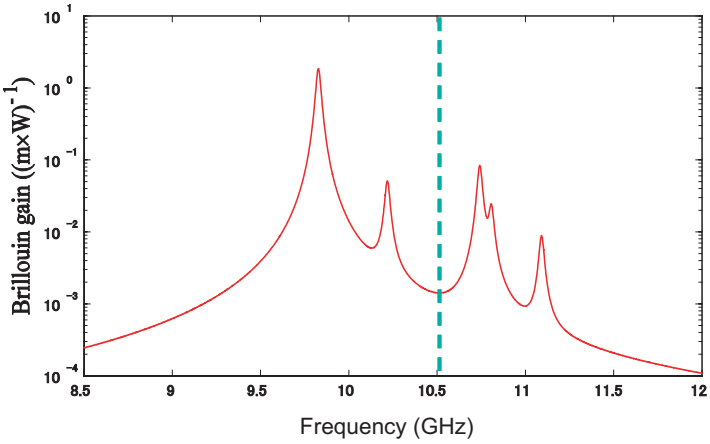

Fig. 7. Simulated BGS in an F-HDF demonstrated by Yeniay *et al.* [8]. A dashed line distinguishes the two groups of BGS in the GeO_2-doped core and the F-doped inner cladding, respectively.

mol% and 10 *mol%*. From it, we know that they match each other within less than 1% difference. This similarity further shows that the distinction of W_{ac}/S between neighboring acoustic modes is almost independent on w_1 for a constant v_{ac}. From Eq. (10) together with Eq. (5) and Eq. (9), we can deduce

$$\nu_{ac}^{(l)} = \frac{2V_{l0}}{\lambda_o}\sqrt{b(n_1^2-n_0^2)+n_0^2-\frac{W_{ac}^{(l)2}/S^2}{4k_0^2a_1^2}}, \tag{14}$$

where $b = W_{op}^2/v_{op}^2$ is the normalized optical propagation constant. The resonance frequency spacing ($\Delta\nu_{ac}^{(l)} \equiv \nu_{ac}^{(l+1)} - \nu_{ac}^{(l)}$) between neighboring longitudinal acoustic modes can be further

#96317 - $15.00 USD Received 16 May 2008; revised 18 Jun 2008; accepted 18 Jun 2008; published 23 Jun 2008

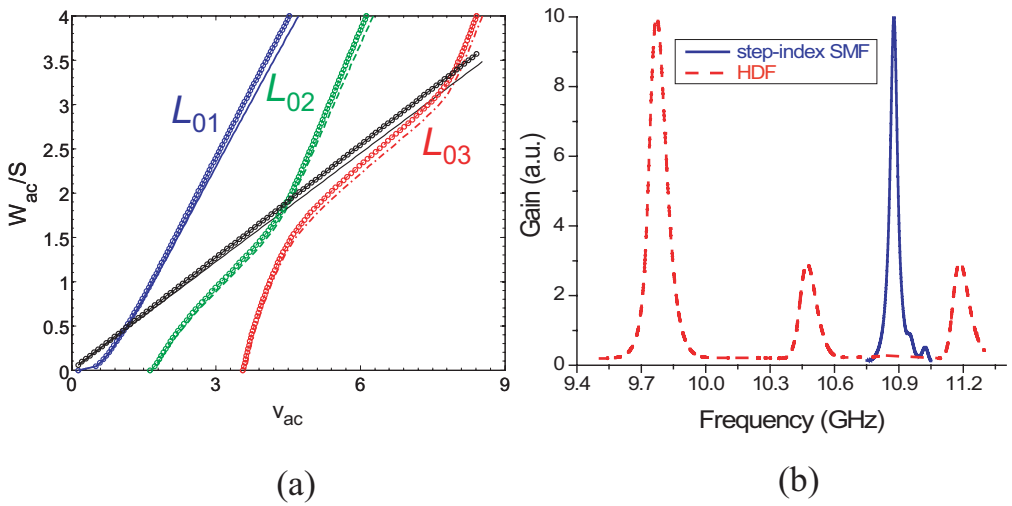

Fig. 8. (a) Acoustic dispersion curves for $w_1 = 3.65$ *mol%* (curves with circle symbols) and $w_1 = 10$ *mol%* (curves without circle symbols) when the concentration ratio $R = 0.05$ and the radius ratio $S = 3.5$. (b) Measured BGS of a 3.65-*mol%* step-index SMF (solid curve) and of a 17.0-*mol%* high-delta fiber (dashed curve).

deduced to be

$$\Delta\nu_{ac}^{(l)} \simeq \frac{1}{\nu_{ac}^{(l)}} \frac{V_{l0}^2}{\lambda_0^2} \frac{W_{ac}^{(l)2}/S^2 - W_{ac}^{(l+1)2}/S^2}{2k_0^2 a_1^2}. \tag{15}$$

According to the definition of v_{ac} in Eq. (9), for a fixed v_{ac} meaning a fixed v_{op} and b approximately, an increase of w_1 corresponds to a reduction of the core size a_1 resulting in a smaller resonance frequency $\nu_{ac}^{(l)}$ [see Eq. (14)]. Furthermore, according to Eq. (15), a quadratic increase of the neighboring resonance frequency spacing arises from a increase of w_1 or a reduction of a_1. This is the reason why a high-delta optical fiber (HDF) with highly GeO_2-doped core is preferred in this study since the enlarged frequency spacing is helpful to improve the measurement system performance in discriminative sensing of strain and temperature [7], and is useful to increase the sensitivity of higher-order resonance frequency to the change of the fiber parameters as will be described below.

The above theoretical prediction is experimentally confirmed by measuring the entire BGS in a 3.65-*mol%* step-index SMF and in a 17.0-*mol%* HDF via pump-probe SBS-based experimental configuration [7]. The experimental results are depicted in Fig. 8(b) showing that the neighboring frequency spacing is ~50-60 MHz for the step-index SMF while ~700-720 MHz for the HDF.

4. Application for discriminative sensing

At first, we investigate the possibility of L_{01} and L_{02} acoustic modes for discriminative sensing, for which L_{03} acoustic mode is cutoff by the pure-silica outer cladding and L_{02} acoustic mode is moved into the F-doped inner cladding. Note that the fundamental L_{01} acoustic mode is always located in the GeO_2-doped core since its critical $v_{c-ac}^{(1)}$ is extremely low, such as less than 1.9 as illustrated in Fig. 4, which corresponds to $v_{op} = \sim 0.35$ according to Fig. 2. The modal control conditions can be understood from Fig. 6(a) in which the crossing point decides

#96317 - $15.00 USD Received 16 May 2008; revised 18 Jun 2008; accepted 18 Jun 2008; published 23 Jun 2008

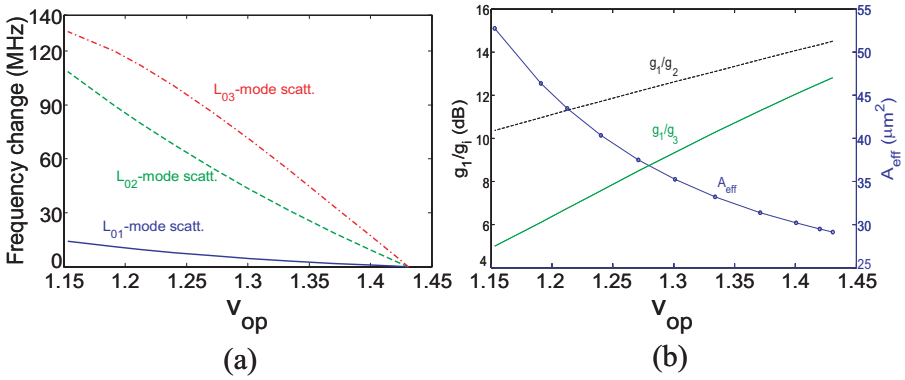

Fig. 9. (a) Each resonance frequency change, and (b) gain ratio (g_1/g_2 and g_1/g_3, respectively) and optical effective area (A_{eff}) as functions of optical v_{op} for $S = 1.5$, $R = 0.05$ and $w_1 = 10\ mol\%$.

a set of R and v_{ac}-value (v_{op}-value correspondingly). A smaller S gives a greater v_{ac}-value or v_{op}-value providing better waveguiding efficiency. In this case, our calculation shows that the v_{op} is necessarily small, for instance, $v_{ac} = \sim 4.82$ (or $v_{op} = \sim 0.85$) and $R = 0.05$ when $S = 2$ and $w_1 = 10\ mol\%$. The corresponding optical effective area defined by

$$A_{eff} = \frac{< E_i^2 >^2}{< E_i^4 >} \tag{16}$$

is evaluated to be $\sim 10^3\ \mu m^2$, which means that the optical waveguiding efficiency in the physical core is extremely weak. In fact, this fiber design is impractical even although the Brillouin gain of L_{02} acoustic mode located in the F-doped inner cladding could be even greater than that of the fundamental L_{01} acoustic mode located in the GeO_2-doped core.

To ensure the optical waveguiding efficiency, we propose to utilize L_{03} acoustic mode together with the fundamental L_{01} acoustic mode for discriminative sensing, for which L_{04} acoustic mode is cutoff by the outer cladding and L_{03} acoustic mode is moved into the inner cladding while L_{01} and L_{02} acoustic modes are maintained in the core. Again, as depicted in Fig. 6(b), a smaller radius ratio S (e.g., = 1.5) is chosen to get a greater crossed v_{ac}-value of ~ 8.12 corresponding to v_{op}-value of ~ 1.43 and a larger $R = 0.05$ when $w_1 = 10\ mol\%$.

Figure 9(a) depicts the analyzed resonance frequencies changing as a function of v_{op} from $v_{op} = 1.43$ to $v_{op} = 1.15$, which corresponds to the range from below the crossed v_{ac}-value (~ 8.12) to beyond the L_{03} mode's cutoff $v_{0ac}^{(3)}$ (~ 5.93). The resonance frequency change of the L_{03} acoustic mode is ~ 7 times as that of the fundamental L_{01} acoustic mode providing a higher sensitivity to the fiber parameter's change. The Brillouin gain ratios (g_1/g_2 and g_1/g_3) and the optical effective area (A_{eff}) are also evaluated and thus plotted in Fig. 9(b), respectively. When v_{op} (v_{ac} correspondingly) decreases, the optical effective area (A_{eff}) increases because the optical confinement is weakened as can be seen from Fig. 5. On the other hand, the Brillouin gain (g_3) of the $3rd$-order L_{03} acoustic mode becomes more comparable to the fundamental L_{01} acoustic mode when compared to the g_2 of the $2rd$-order L_{02} acoustic mode. This is because the displacement field of the $3rd$-order L_{03} acoustic mode enters more into the F-doped inner-cladding region for a smaller acoustic v_{ac} ($< v_{c-ac}^{(3)}$) while the field of L_{02} acoustic mode dominantly confined in the GeO_2-doped core has tiny change with v_{ac} (see Fig. 5). Consequently, comparing to L_{02} acoustic mode, L_{03} acoustic mode has greater acousto-optic overlapping efficiency with the weakly-guided LP_{01} optical mode.

#96317 - $15.00 USD Received 16 May 2008; revised 18 Jun 2008; accepted 18 Jun 2008; published 23 Jun 2008

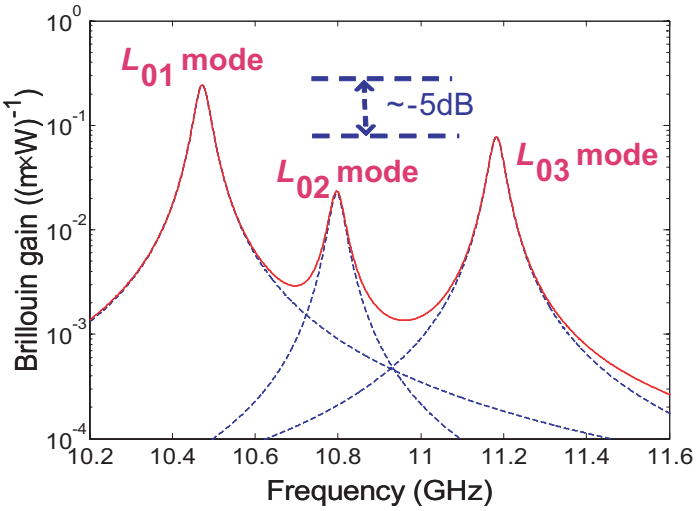

Fig. 10. Simulated BGS in an optimally-designed fiber for application of L_{01} and L_{03} acoustic modes in discriminative sensing. Note that its optical effective area (A_{eff} = 53 μm^2) is comparable to that of a standard SMF ($\sim$80 μm^2) and the Brillouin gain of L_{03} acoustic mode is only $\sim$-5 dB lower than that of L_{01} mode.

Furthermore, these analyzed results show a feasibility of utilizing L_{01} and L_{03} acoustic mode for discriminative sensing of strain and temperature by choosing v_{op} = 1.15 or v_{ac} = 6.53. Firstly, A_{eff} can be kept to be as low as $\sim$53 μm^2. Secondly, the simulated BGS of the optimized fiber design illustrated in Fig. 10 shows that the Brillouin gain of L_{03} acoustic mode is only $\sim$-5 dB lower than that of the fundamental L_{01} acoustic mode. This is because the acoustic v_{ac} = 6.53 is very close to the L_{03} acoustic mode's cutoff $v_{0ac}^{(3)}$ = $\sim$5.93, so that the existence of the L_{03} acoustic field in the F-doped inner cladding is significantly enhanced (see Fig. 5(d)).

5. Conclusions

We have demonstrated the theoretical and numerical analysis of optical and acoustic modal properties in the F-HDF including cutoff conditions and acoustic dispersion curves. With appropriately designed parameters (radii and dopant concentrations), we can put the L_{03} longitudinal acoustic mode into the F-doped inner cladding effectively with comparable Brillouin gain in contrast with the fundamental L_{01} longitudinal acoustic mode and with more sensitive change ($\sim$6 times) of the resonance frequency than that of the fundamental L_{01} mode. When the L_{01} and L_{03} resonance BGS in the optimally designed F-HDF are utilized for fiber-optic Brillouin sensors, an improvement of our preliminarily investigated accuracy of discriminative measurement of strain and temperature (e.g., strain error of 44 $\mu\varepsilon$ and temperature error of 1.8 ^{o}C [7]) is hopefully achievable.

6. Acknowledgment

This work was supported by the "Grant-in-Aid for Creative Scientific Research" and the "Global Center of Excellence Program (G-COE)" from the Ministry of Education, Culture, Sports, Science and Technology, Japan.

#96317 - $15.00 USD Received 16 May 2008; revised 18 Jun 2008; accepted 18 Jun 2008; published 23 Jun 2008